JOURNAL OF CATALYSIS 51, 229–242 (1978)

Chemisorption of Hydrogen Sulfide on Nickel and Ruthenium Catalysts

I. Desorption Isotherms

JOSEPH L. OLIPHANT, RICHARD W. FOWLER, RICHARD B. PANNELL, AND CALVIN H. BARTHOLOMEW

Department of Chemical Engineering, Brigham Young University, Provo, Utah 84602

Received July 12, 1977; revised October 21, 1977

Desorption isotherms for H_2S on unsupported nickel and alumina-supported nickel, nickel–platinum, nickel–cobalt, and ruthenium were calculated from elution curves of H_2S from a packed bed of each catalyst. All elution experiments were run initially at 450°C and at H_2S concentrations in the exiting hydrogen stream from 30 to 0.1 ppm. Elution curves and isotherms for supported nickel–platinum were also obtained at 450 and 520°C from which an estimate of the heat of H_2S chemisorption was calculated. The heat of H_2S adsorption on nickel is estimated to be 30–40 kcal/mole at 450°C and high coverage (50–90%). The stoichiometry of sulfur adsorption was determined by comparing the total quantity of sulfur adsorbed at 450°C with the corresponding quantity of hydrogen chemisorbed at 25°C for each catalyst. The data suggest that H_2S chemisorption is strong and dissociative at low coverage and nondissociative at high coverages. Ruthenium apparently has a lower capacity for sulfur adsorption than nickel or nickel alloys.

INTRODUCTION

Poisoning of metallic catalysts by hydrogen sulfide and other sulfur-containing compounds in extremely low concentrations is a major problem in hydrogenation reactions, such as methanation of coal synthesis gas (*1*, *2*). Methods used to attain low sulfur concentrations and/or longer catalyst life include: (i) purification of the synthesis gas to remove sulfur, (ii) installation of guard chambers to adsorb sulfur compounds, and/or (iii) installation of excess catalyst to allow for sulfur adsorption. Each of these methods suffers significant economic limitations. Thus, there is considerable economic incentive to find a catalyst with relatively high methanation activity in the presence of 1–10 ppm H_2S. Unfortunately, the steady-state activity of supported nickel in 10 ppm H_2S is much too low (*3*). This behavior undoubtedly relates to the manner in which H_2S adsorbs on nickel.

Previous work (*4–6*) suggests that the surface nickel–sulfur bond is more stable than the bulk nickel–sulfur bond, but the adsorption is nevertheless reversible (*5*). For example, in his work on the sulfiding of Kieselguhr-supported nickel catalysts, Richardson (*6*) found that if the nickel was completely sulfided by relatively large concentrations of H_2S in the bulk-sulfide-forming region (*7*), the bulk sulfur could be removed by reaction with pure hydrogen. The surface sulfur, apparently, could not be easily removed, as the catalytic activity was not restored.

Assuming that the surface nickel sulfide is more stable than bulk sulfides, the heat

0021-9517/78/0512-0229$02.00/0

of adsorption should be larger in magnitude than the heats of formation for bulk phases. However, estimates for the heat of adsorption of H_2S on nickel from Perdereau and Oudar (*4*), Roberts (*8*), and Rostrup-Nielsen (*9*) range from 10 to 50 kcal/mole. Since the enthalpy of adsorption is in doubt, entropy of adsorption data for H_2S on nickel are also lacking.

There are also apparent discrepancies regarding mechanisms of H_2S adsorption on metals, although it is generally reported to be dissociative. Den Besten and Selwood (*10*) inferred from magnetochemical measurements at 0–115°C that H_2S forms four bonds with the nickel surface:

$$H_2S_{(g)} + \text{–Ni–Ni–Ni–Ni–} \rightarrow$$

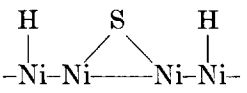

They also found that at high coverages sulfur displaces hydrogen from the surface. Saleh *et al.* (*11*) suggested a three-site mechanism in the temperature range 80 to 100°C, whereas Rostrup-Nielsen (*5*) suggested a one-site mechanism at 550 to 645°C,

$$H_2S_{(g)} + Ni_{(s)} \rightarrow Ni\text{–}S_{(s)} + H_{2(g)},$$

based on the value of one obtained for the power, n, in a Langmuir fit for his data.

There is apparently only fair agreement as to the stoichiometry of H_2S adsorption on nickel. Saleh *et al.* (*11*) reported that H_2S readily displaced adsorbed hydrogen from nickel films at −80°C, and that one molecule of the sulfide covered the same surface area as three atoms of hydrogen or one atom of krypton. Selwood's mechanism suggests one H_2S molecule adsorbing (at 25°C) per four nickel atoms (*10*). Rostrup-Nielsen (*5*) calculated a value of 0.54 sulfur atoms per nickel atom at 550–645°C.

In this paper, desorption isotherms of H_2S on Ni, Ni–Co, Ni–Pt, and Ru catalysts determined at 450°C and isosteric heats of adsorption of H_2S on Ni and Ni–Pt (450–520°C) are presented and discussed. The application of these data in determining the stoichiometry and mechanism of H_2S adsorption on metals and supports is also discussed.

EXPERIMENTAL METHODS

Materials

Three grams of a high-purity carbonyl nickel powder (Inco) initially containing less than 1 μg/g of sulfur were reduced at 450°C for 2 hr, and the H_2 chemisorption isotherm was measured before poisoning.

Supported nickel and nickel–alloy catalysts were all prepared in this laboratory by impregnation to incipient wetness using Kaiser alumina beads having a surface area of 301 m^2/g. A large batch of each catalyst was reduced and passivated according to procedures described previously (*12*). The ruthenium catalyst (Engelhard Industries) was received in a reduced and passivated state. All supported catalysts were crushed to a powder before use in the poisoning experiments to minimize mass transfer effects. A sample of each previously reduced and passivated catalyst was analyzed for initial sulfur content. Separate samples of each catalyst were re-reduced at 450–500°C for 2 hr, following which their H_2 chemisorption isotherms were measured at room temperature before poisoning. Table 1 gives the nominal composition and initial H_2 uptake for each catalyst.

Hydrogen (99.995%) was purified using an Engelhard industries Deoxo catalyst followed by a molecular sieve trap. The H_2S in H_2 calibration mixture was prepared by Matheson.

Procedure

Sample poisoning and H_2S elution curves. H_2 adsorption isotherms were measured at 25°C using an apparatus and procedure described earlier (*12*). Samples were heated

TABLE 1

Sulfur Atom vs Hydrogen Atom Uptakes

Catalyst	H atom uptake at 25°C (μmoles/g of sample)	Saturation, S atom uptake at 450°C (μmoles/g of sample)	S/H	H_2S concentration (ppm)
3% Ni/Al_2O_3	80.0	86.5	1.08	25
3% Ni/Al_2O_3	80.0	68.5	0.86	8
3% Ni/Al_2O_3	80.0	60.4	0.76	12
Nickel powder (Inco)	3.71	4.23	1.14	23
10% Ni–10% Co/Al_2O_3	229.8	205.9	0.90	25
16% Ni–0.5% Pt/Al_2O_3	229.0	194.0	0.85	25
Ruthenium (Engelhard) (0.5% Ru/Al_2O_3)	22.0	8.53	0.39	25
Alumina support	1.0	4.4	—	25

to 450°C in flowing hydrogen and then exposed to a gas mixture containing 8 to 30 ppm H_2S in H_2, provided by combining pure H_2 with a gas stream containing 120 ppm H_2S in H_2. The flow rate of gas through the samples was about 255 ml/min (measured at room temperature and 640 Torr, 1 Torr = 133.3 nm^{-2}). The concentration of H_2S in the gas was measured for both entering and exiting streams of the catalyst bed. When the H_2S concentrations of the entering and exiting gas streams were the same (usually after 16–24 hr), it was assumed the catalyst was saturated with sulfur.

After the catalyst was saturated with sulfur, pure hydrogen was passed through the sample at a rate of 200 ml/min. The

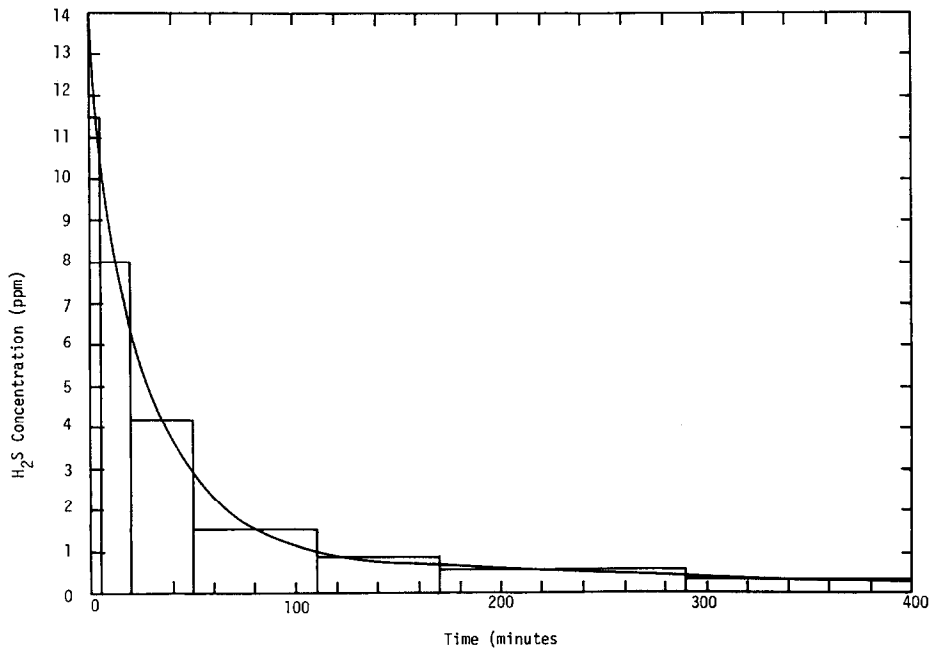

FIG. 1. H_2S elution curve for pure nickel.

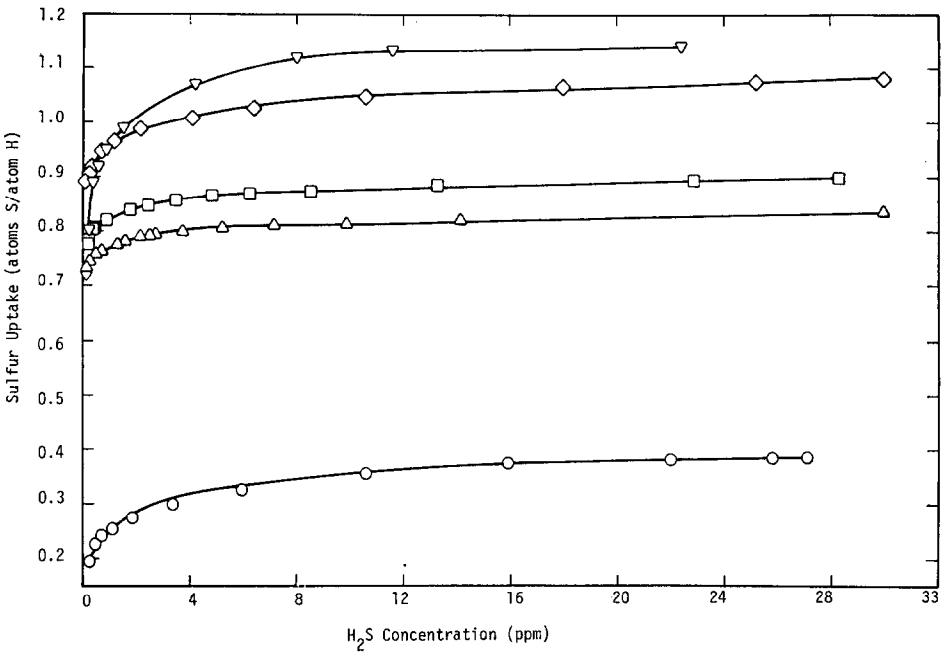

FIG. 2. H_2S desorption isotherms at 450°C normalized to H_2 uptake: (◇) 3% Ni; (▽) Ni powder; (△) Ni–Pt; (□) Ni–Co; (○) Ru.

H_2S leaving the bed via the H_2 stream was collected continuously and analyzed periodically so that an elution curve of H_2S concentration versus time could be made for each sample. Desorption isotherms were obtained from the elution curves using the method of characteristics (*13*, *14*, Appendix).

In addition, individual catalyst samples were exposed over long periods (16–24 hr) to H_2S (in H_2) at concentrations ranging from 3 to 25 ppm to establish single equilibrium points in the same manner as Rostrup-Nielsen (*5*) for comparison with the desorption isotherms obtained from the elution curves.

Sulfur analysis. Gas-phase hydrogen sulfide was analyzed colorimetrically by absorption in a cadmium acetate solution followed by reaction to form methylene blue according to Zutshi and Mahadevan (*15*). Catalysts were analyzed for sulfur content by reducing the sulfur to hydrogen sulfide according to Gustafsson (*16*, *17*), then absorbing the H_2S removed by a N_2 purge stream, and finally carrying out the color reaction to methylene blue as indicated above.

RESULTS

Hydrogen sulfide elution curves were obtained for each sample at 450°C; an additional elution curve was obtained for Ni–Pt at 520°C. The elution curve for the unsupported nickel sample is shown in Fig. 1 and evidences exponential decay. Using the method of characteristics (see Appendix), the elution curves were transformed into H_2S desorption isotherms. The isotherms were normalized to the initial hydrogen uptakes of each catalyst and are presented in Fig. 2 in terms of atoms of adsorbed sulfur per atom of adsorbed hydrogen. Saturation levels of adsorbed sulfur and S/H ratios at saturation were determined for each sample from the linear portions of the desorption isotherms (above 10–25 ppm) and are tabulated in Table 1. The saturation sulfur coverages were calcu-

lated for each sample by adding the total amount of sulfur eluted from the bed to the amount remaining on the catalyst in the bed. The small amount of sulfur initially present in each unpoisoned supported catalyst was assumed to play a negligible role in the desorption isotherm and was subtracted from the initial coverage for each sample.

The experimental desorption isotherms (Fig. 2) appear to follow an equation of the Langmuir form,

$$\theta = (bp)^{1/n}[1 + (bp)^{1/n}]^{-1}.$$

To find the value of n, this equation can be linearized to the following form:

$$\ln (q/q_0 - q) = \ln b' + 1/n \ (\ln p).$$

In this equation p is the partial pressure of H_2S in the gas phase, $\theta = q/q_0$ is the coverage of sulfur on the surface, and $b' = (b)^{1/n}$. The value chosen for q_0 in the above equation was found to depend to a small degree upon the method of extrapolation, but in all cases was only slightly greater than the coverage at 25 ppm because the isotherms are fairly flat in this region. To obtain consistent values of q_0 each data set was linearized by plotting $\ln [\ln (q/q_0 - q)]$ versus $\ln p$ and extrapolating to the high $\ln p$ range; this q_0 value was then used to calculate n by linear regression analysis.

Figure 3 shows plots of $\ln (q/q_0 - q)$ versus $\ln p$ for each sample run. For the nickel catalysts the data points obtained at the lower partial pressures of H_2S (i.e., at lower values of H_2S surface coverage, q) show a Langmuirian fit with a slope approximately equal to one-third; at higher

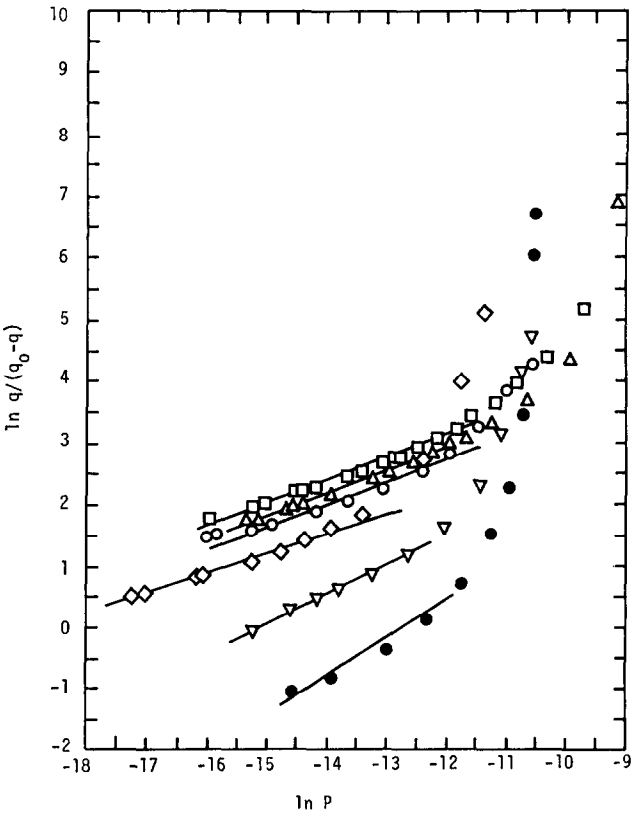

FIG. 3. Langmuir curve fits of H_2S desorption isotherms. (□) Ni–Pt; (▽) Ru; (△) Ni–Co; (○) Ni/Al_2O_3; (◇) pure Ni; (●) Al_2O_3.

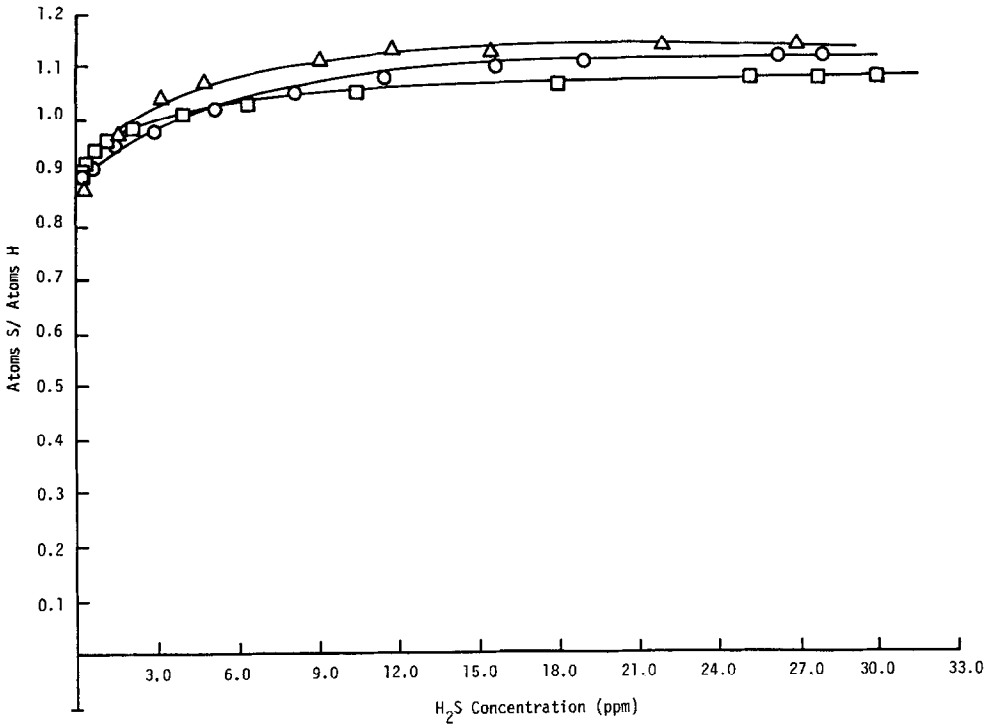

FIG. 4. Effects of hydrogen flow rate on hydrogen sulfide adsorption on 3% Ni/Al_2O_3: (○) 100 ml/min; (□) 200 ml/min; (△) 400 ml/min.

pressures (2–5 ppm) the slope increases to slightly greater than one. For the Al_2O_3 support and supported ruthenium the slope is approximately one-half at low pressures, also increasing to one at higher pressures.

Since the assumption of local equilibrium in the catalyst bed is requisite for the analytical method of characteristics, the effects of hydrogen flow rate on hydrogen sulfide elution curves were studied. Hydrogen was passed at three different flow rates over samples of 3% Ni/Al_2O_3, each of which had been previously saturated at H_2S concentrations of approximately 25–30 ppm. Hydrogen flow rates of 100, 200, and 400 ml/min were used and the differences in uptake versus concentration, as shown in Fig. 4, were found to be negligible within experimental error; hence, the assumption of equilibrium in the bed was considered valid and a flow rate of 200 ml/min was used throughout the remainder of the study.

To determine the effect of H_2S concentration on the sulfur saturation level, H_2S desorption isotherms for identical samples of 3% Ni/Al_2O_3 catalyst were determined at H_2S concentrations of 8, 12, and 30 ppm and individual equilibrium adsorption points (each for a different sample of 3% Ni/Al_2O_3) were determined at various concentrations between 3 and 25 ppm. The data are represented graphically in Fig. 5 and saturation coverages are tabulated in Table 1. Comparison of data at 8 and 12 ppm with those at 30 ppm shows that saturation sulfur coverage increases with increasing concentration of H_2S in the gas phase. Good agreement is observed for the single adsorption points below 10 ppm compared to the desorption data for samples saturated at 8 and 12 ppm.

To obtain an estimate of the adsorption heat of H_2S on Ni–Pt, the elution of H_2S was carried out at 450°C until an exit H_2S

gas concentration of about 0.1 ppm was achieved; then the H_2 flow was shut off. The sample cell was heated further to 520°C and the elution curve was continued to enable several more data points to be collected. The results are shown in Fig. 6. It can be seen that if both curves are extended slightly to a value of about 5400 μg/sample that two different pressures at the same coverage are obtained corresponding to the two temperatures of the isotherm. At this point the pressures are about 0.10 and 1.0 ppm. Putting these values into the Clausius–Clapeyron equation,

$$\ln (P_1/P_2) = Q/R(1/T_2 - 1/T_1),$$

gives a heat of adsorption, Q, of about 38 kcal/mole.

In Fig. 7, log (P_{H_2S}/P_{H_2}) values for nickel and nickel–platinum catalysts are plotted versus reciprocal temperature and compared with previously reported data (*4*, *5*) for H_2S adsorption on Ni. The solid line corresponds to the equilibrium data reported by Rosenqvist (*7*) for formation of Ni_3S_2 (in the temperature range 400–535°C). Based on the Clausius–Clapeyron equation the slope of this line corresponds to an enthalpy of −18.0 kcal/mole. The dashed lines in Fig. 2 represent equilibrium lines for chemisorbed sulfur with heats of adsorption of 20, 30, and 40 kcal/mole, assuming formation of Ni_3S_2 (i.e., the same intercept as the solid line for Ni_3S_2). Thus, according to these data in Fig. 7, the enthalpy of adsorption of H_2S on nickel is 10 to 20 kcal/mole more exothermic than the heat of formation of Ni_3S_2 depending upon temperature and coverage. It is also apparent that the absolute value of the heat increases with decreasing coverage and that the equilibrium partial pressure of H_2S increases with increasing temperature.

From the estimate for the enthalpy of adsorption of H_2S on nickel (or nickel–platinum) it is possible to calculate an

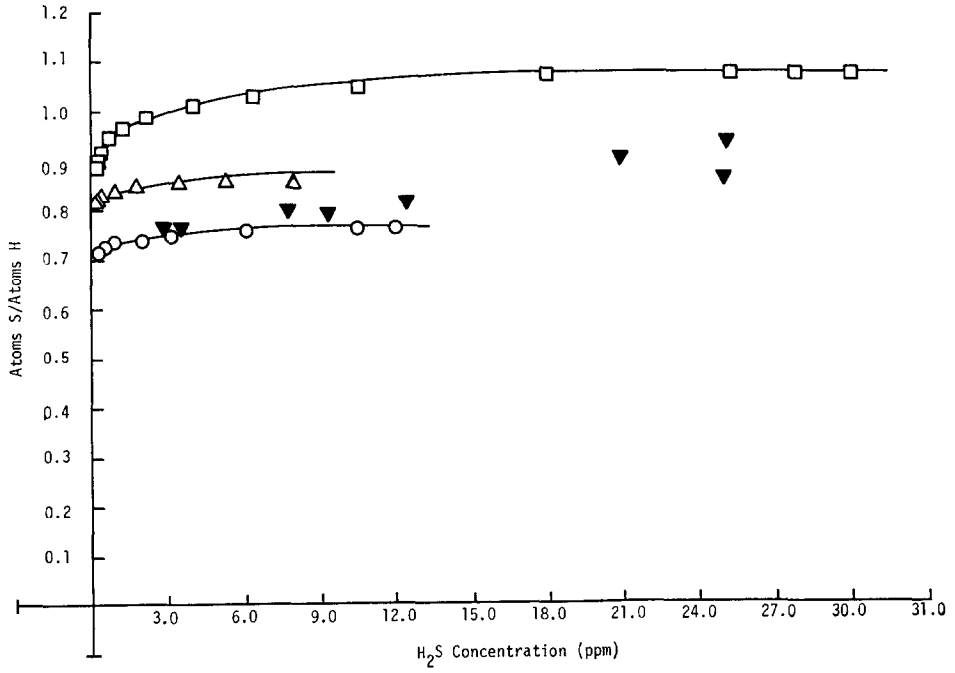

FIG. 5. Effect of hydrogen sulfide concentration on hydrogen sulfide adsorption on 3% Ni/Al_2O_3. (□) Desorption isotherm data after saturation at 30 ppm; (○) desorption isotherm data after saturation at 12 ppm; (△) desorption isotherm data after saturation at 8 ppm; (▼) single equilibrium adsorption points.

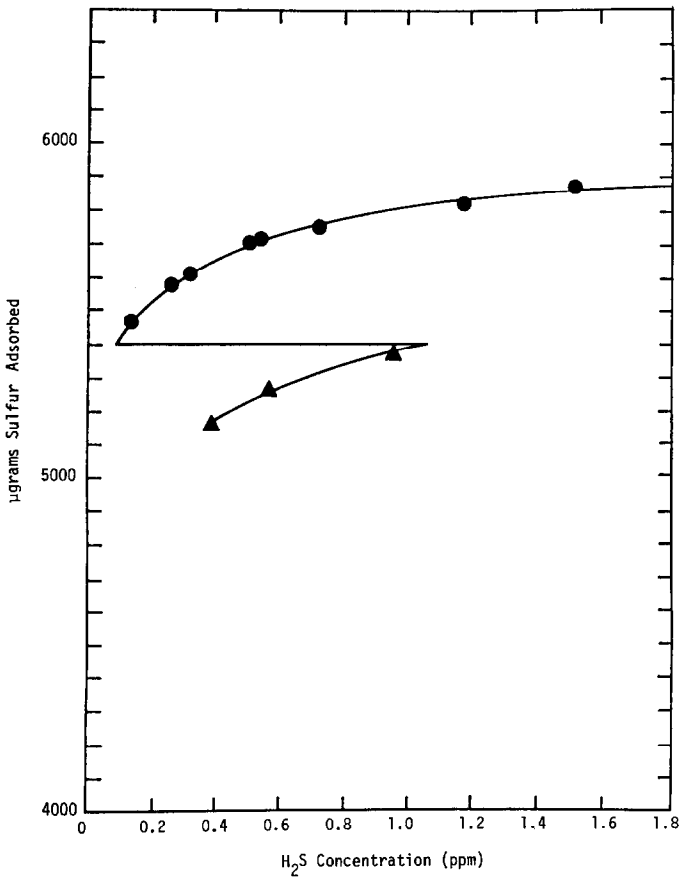

FIG. 6. Ni–Pt desorption isotherms at 450°C (●) and 520°C (▲).

entropy of adsorption from the relation $\Delta G = \Delta H - T\Delta S$, where $\Delta G^\circ = RT \ln (P^\circ/P)$ and $P^\circ = 1$ atm H_2S. For unsupported Ni the entropy of H_2S adsorption at 450°C and a coverage of 50% is estimated to be −7.2 e.u. (cal/°K gmole) based upon an enthalpy of −32 kcal/mole of H_2S (from Fig. 7) and a free energy of −26.8 kcal/mole. For nickel–platinum the entropy of adsorption at 450°C and $\theta = 0.50$ was determined to be −10.8 e.u. based on a ΔH value of −38.0 kcal/mole and a ΔG° value of −30.2 kcal/mole.

DISCUSSION

The H_2S desorption isotherms in Fig. 2 illustrate the *equilibrium* adsorption behavior for nickel, nickel bimetallics, and ruthenium at 450°C. The shapes of these curves show that adsorption is very strong and that moderately low coverages (i.e., 30–50%) are observed at only very low H_2S concentrations (i.e., less than 0.1 to 1 ppm). The assumption of equilibrium is supported by (i) the data for 3% Ni/Al_2O_3 in Fig. 4 showing the coverage to be independent of flow rate and (ii) the data in Fig. 5 showing very good agreement between the desorption curves and the adsorption points in the range of 3–12 ppm H_2S.

The H_2S desorption isotherms normalized to the H_2 uptake for each sample (see Fig. 2 and Table 1) give direct information regarding the stoichiometry of H_2S adsorption as a function of concentration. For most of the catalysts, saturation coverage

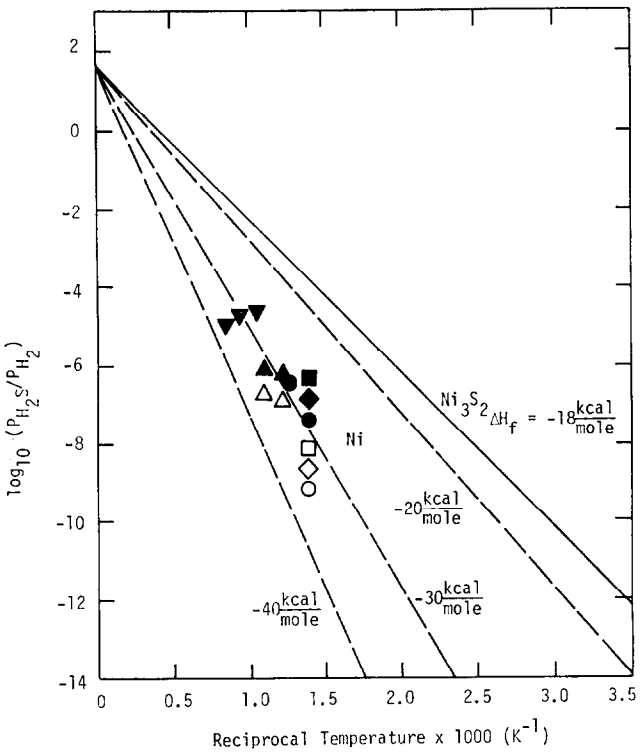

FIG. 7. Equilibrium partial pressure of H_2S versus reciprocal temperature. (□) Ni powder, this study; (◇) 3% Ni/Al_2O_3, this study; (○) 16% Ni, 0.5% Pt/Al_2O_3, this study; (△) 10% Ni/MgO–Al_2O_3, Ref. (*5*); (▽) Ni foil, Ref. (*4*). Closed symbols, $\theta = 0.50$; open symbols, $\theta = 0.80$.

is nearly complete around 5 ppm H_2S, and the further increase in sulfur uptake with increasing concentration above 5 ppm is relatively small. At a concentration of 25 ppm (see Table 2) the S/H ratios are 1.08 and 1.14 for 3% Ni/Al_2O_3 and pure nickel, respectively. After correction for sulfur uptake by the alumina support and based upon a H/Ni_s stoichiometry of 1:1, the S/Ni_s value for 3% Ni/Al_2O_3 is 1.04. Similarly, the S/Ni_s stoichiometries for saturation at 8 and 12 ppm H_2S (after correcting for the support) are 0.83 and 0.73. These values of the S/Ni ratio are two to four times greater than values reported by Den Besten and Selwood (*10*) at 25°C and Saleh *et al.* (*11*) at −78°C, and 50–100% larger than the value of 0.54 reported by Rostrup-Nielsen (*5*) for the temperature range 550–645°C. A priori, it is reasonable to expect that at most about 0.6 to 0.7 atoms of sulfur chemisorb on a clean nickel surface in view of the relative areas of about 10 and 6.5 Å²/atom (10 Å = 1 nm) for S and Ni atoms, respectively.

These apparent discrepancies can be resolved as follows. First, the values of 0.25 and 0.33 atoms of sulfur per nickel surface atom (*10*, *11*) are observed at the lower temperatures because the hydrogen atoms from the dissociative chemisorption of H_2S bond irreversibly with nickel sites, preventing further sulfur adsorption. Since at higher temperatures the chemisorption of hydrogen is reversible, sulfur atoms can cover most or all of the nickel sites, and thus higher S/Ni_s ratios are possible. Moreover, the value of S/Ni_s of 0.54 reported by Rostrup-Nielsen for 10% Ni/Al_2O_3 (550–645°C) is based on the assumption of $H/Ni_s = 0.73$. Recent data from this laboratory (*18*) have shown that the correct

TABLE 2

Langmuir Isotherms[a]

Catalyst	Langmuir isotherm
3% Ni/Al_2O_3	$q = 2697 \frac{(2.794 \times 10^8 p)^{1/2.72}}{1 + (2.794 \times 10^8 p)^{1/2.72}}$
Ni powder (Inco)	$q = 135 \frac{(1.270 \times 10^8 p)^{1/2.94}}{1 + (1.270 \times 10^8 p)^{1/2.94}}$
$Ni–Co/Al_2O_3$	$q = 6750 \frac{(5.853 \times 10^8 p)^{1/2.88}}{1 + (5.853 \times 10^8 p)^{1/2.88}}$
$Ni–Pt/Al_2O_3$	$q = 5908 \frac{(1.313 \times 10^9 p)^{1/2.95}}{1 + (1.313 \times 10^9 p)^{1/2.95}}$
Ru/Al_2O_3 (Engelhard)	$q = 275 \frac{(4.027 \times 10^6 p)^{1/2.24}}{1 + (4.027 \times 10^6 p)^{1/2.24}}$
Al_2O_3 (Kaiser)	$q = 170 \frac{(2.561 \times 10^5 p)^{1/1.93}}{1 + (2.561 \times 10^5 p)^{1/1.93}}$

[a] All samples run at 450°C and reported on a per gram basis; q has units of micrograms per gram of catalyst.

stoichiometry is $H/Ni_s = 1.0$. On this latter basis the data of Rostrup-Nielsen are consistent with a value of $S/Ni_s = 0.74$ and in good agreement with the values of 0.83 and 0.73 for 3% Ni/Al_2O_3 at 8 and 12 ppm and with the value of 0.82 for 16% $Ni–Pt/Al_2O_3$ determined at 25 ppm. Furthermore, a S/Ni_s ratio of 0.74 was obtained for the same Ni–Pt sample at a higher temperature (520°C), indicating that H_2S adsorption is more reversible and that the saturation coverage is less at higher temperatures. Hence, the lower saturation coverages obtained by Rostrup-Nielsen at 550–645°C may be due in part to effects of higher temperature.

The larger values of S/Ni_s observed for both supported and unsupported nickel upon desorption after saturation at 25–30 ppm compared to the values after saturation at 8–12 ppm may be explained by (i) a surface reconstruction in the higher concentration range, or (ii) incorporation of S into nickel layers below the surface or into the support. In accordance with the first hypothesis, at H_2S concentrations less than 10 ppm, atomic sulfur is chemisorbed upon the nickel surface up to a coverage of $S/Ni_s = 0.7–0.8$, consistent with Ni_3S_2 stoichiometry; however, saturation at 25–30 ppm with subsequent desorption is accompanied by a reconstruction of the surface to a surface sulfide of nickel consistent with NiS stoichiometry. Apparently this or a similar phenomenon results in a hysteresis effect for adsorption and desorption, as observed in Fig. 5, by a large difference between the desorption isotherm data after saturation at 30 ppm and the adsorption data points from 3 to 12 ppm. Apparently there is also a trend of increasing saturation coverage for the single equilibrium adsorption points with increasing H_2S concentration which almost completes the hysteresis loop.

The hypothesis of reconstruction of the nickel surface by adsorbed sulfur finds considerable support in the literature. Somorjai (*19*) suggested that adsorbed sulfur on platinum causes reconstruction to a new equilibrium distribution of crystallographic planes having less activity. In three different LEED studies of sulfur on nickel (20–22), reconstruction of the (110) and (111) surfaces was observed as the coverage was increased above one-third to one-half. In fact, two different reconstructions were observed on the (111) surface.

It is expected that the extent of reconstruction and the capacity of H_2S adsorption on the nickel surface might be influenced by the presence of supports, promoters, alloying atoms, and by the range of metal crystallite sizes affecting the distribution of crystallographic planes and edge and corner sites. These influences may explain the lower sulfur capacities of nickel bimetallics relative to supported nickel and the different isotherm shapes observed for well-dispersed, supported nickel and poorly dispersed, unsupported nickel.

Since X-ray diffraction data for the Ni–Pt and Ni–Co catalysts provide evidence for the presence of Ni–Pt and Ni–Co alloys (*23*), these catalysts may demonstrate the effects of alloying on sulfur capacity. How-

ever, the Ni–Pt catalyst contains only 1 atomic % Pt and calculations suggest that the surface should be very rich in nickel (*24*); hence the Ni–Pt surface would be expected to behave similar to a nickel surface. Nevertheless, it has been shown that very small amounts of platinum enhance the reduction of nickel to the metallic state (*25*). Perhaps the platinum also stabilizes the nickel in such a way as to minimize reconstruction of the surface when sulfur is adsorbed. The cobalt might play a similar role in the Ni–Co catalyst, although the surface composition of Ni–Co is expected to be about 50 atomic % cobalt (*24*) and Auger measurements (*26*) have shown this to be true.

In comparison with the supported nickel catalysts, the unsupported nickel powder sample evidences more reversible H_2S adsorption at low partial pressures of H_2S, as shown in Fig. 2. In other words, the monolayer coverage of sulfur is completed at a lower partial pressure of H_2S on supported nickel, indicating that small, supported crystallites of nickel adsorb sulfur more strongly.

The data in Fig. 2 and Table 1 showing ruthenium to have approximately one-third to one-half as much sulfur capacity as the nickel catalysts possibly explain the greater susceptibility of ruthenium catalysts to sulfur poisoning (*3*, *27*, *28*). However, because these data are based upon only one sample the results should be interpreted with caution, particularly because the fresh sample had an unusually low activity for methanation (*28*) and may have been contaminated with hydrogen chloride during its preparation.

For all catalysts except alumina and ruthenium the slope of the linear, low coverage portion of each Langmuir isotherm as shown in Fig. 3 is approximately equal to one-third, which is equivalent to a value of $n = 3$ in the Langmuir equation. This suggests that upon adsorption at the lower coverages, H_2S dissociates into three species covering three adsorption sites:

$$H_2S_{(g)} + -Ni-Ni-Ni- \rightarrow \begin{matrix} H & S & H \\ | & | & | \\ -Ni- & Ni- & Ni- \end{matrix}$$

The value of $n = 2$ for ruthenium and alumina suggests that partial dissociation of H_2S is the more prevalent mechanism for adsorption on these samples. The high-pressure portion of each curve (in Fig. 3) where n equals one is consistent with non-dissociative adsorption of H_2S on sites of lower energy.

The proposed two- or three-site mechanism for dissociative adsorption is in agreement with the previous work on nickel by Den Besten and Selwood (*10*) at 25°C and on alumina by Glass and Ross (*29*). The latter workers observed dissociative adsorption of H_2S on alumina at low coverages. Our Langmuir exponent of one-third for nickel at 450°C does not agree with the value of one determined by Rostrup-Nielsen (*5*) at 550–645°C. This disagreement possibly stems from the differences inherent in the adsorption and desorption techniques, the latter involving less scatter in the isotherm data.

The value of 38 kcal/mole for the isosteric heat of H_2S adsorption on nickel–platinum at 450–520°C and a coverage of about 85% and the heats of adsorption for nickel of 30–35 kcal/mole for $\theta = 0.5$ (from Fig. 7), although somewhat approximate, establish that H_2S chemisorption on nickel is very strong even at high coverages.

The thermodynamic data for the Ni–Pt catalyst are believed to be applicable to supported nickel in a highly reduced state (*25*) because the metal contains only 1 atomic % Pt and the surface composition is most likely very rich in nickel (*24*). This is confirmed by the close proximity of data for Ni and Ni–Pt in Fig. 7.

The adsorption stoichiometries of 0.7–0.8 observed at 8–12 ppm H_2S for 3% Ni/Al_2O_3 are consistent with the formation of a Ni_3S_2 surface structure. This observation finds support from the LEED studies of Perdereau and Oudar (*4*), who observed a

surface structure very similar to Ni_3S_2. Demuth *et al.* (*30*), however, observed Ni–S bond lengths shorter than the nearest-neighbor distance in Ni_3S_2 and more characteristic of NiS. Perhaps the discrepancy in the two LEED studies stems from reconstruction effects at different coverages.

The differences in heats of adsorption for the supported Ni, unsupported Ni, and Ni–Pt catalyst may possibly be a result of support and extent of reduction effects. They suggest, for example, that H_2S adsorbs most strongly on highly reduced, supported nickel and least strongly on unsupported nickel. Certainly, more experimental work is needed to confirm if these effects are significant.

The gas-phase entropies of H_2S and H_2 at 450°C (reference states at 1 atm) are 56.9 and 37.4 cal/mole °K, respectively (*31*). Accordingly, the predicted entropy change between H_2 and H_2S is -19.5 cal/mole °K. Thus, the experimental entropy change of 7–10 e.u. for H_2S adsorption on Ni and Ni–Pt is less than the predicted entropy change $S_{H_2} - S_{H_2S}$. This difference may be explained in a number of ways. For example, the entropy difference between empty and occupied or rearranged sites may account for this difference. Alternatively, the experimental heat of adsorption is expected to increase with decreasing coverage and this would result in a larger entropy decrease more in line with the prediction.

CONCLUSIONS

1. H_2S chemisorption on nickel and ruthenium catalysts is very strong even at high coverages. Values of the heat of H_2S adsorption on nickel are estimated to be 30–40 kcal/mole at surface coverages of 50–90%. This heat of adsorption includes heats for dissociation and adsorption of 2H and S.

2. H_2S chemisorption on nickel at 450°C is dissociative in the range of low to monolayer surface coverages (up to about 0.8–0.9 S atoms/H atom). At higher coverages H_2S may adsorb as molecular H_2S.

3. If H_2S is desorbed after saturation at gas-phase concentrations of 25–30 ppm there is apparently a reconstruction of the surface consistent with Ni–S stoichiometry. For saturation at 8–12 ppm H_2S the surface stoichiometry is consistent with Ni_3S_2. Agreement is observed between adsorption and desorption data in the lower concentration range (8–12 ppm).

4. Well-dispersed, supported nickel catalysts show a tendency to adsorb H_2S more strongly than the unsupported nickel powder. Ni–Co and Ni–Pt catalysts have lower saturation coverages than nickel catalysts. These differences may be attributed to alloying, support, and crystallite size effects.

5. Supported ruthenium (0.5% Ru/Al_2O_3) has a much lower capacity for H_2S adsorption than supported nickel catalysts.

6. The determination of equilibrium data from desorption isotherms has the following advantages relative to the adsorption techniques previously used: (i) The desorption data can be obtained more quickly (2–3 days compared to 8–10 days for adsorption isotherms), and (ii) the desorption isotherms evidence considerably less scatter because the desorption data are determined from a single sample, whereas a separate sample is used for each point in the adsorption technique. The equilibrium data obtained from desorption isotherms at high surface coverages have practical value because in most catalytic processes involving H_2S as a poison, the surface is likely to be nearly saturated with H_2S. Unfortunately, the data show that removal of H_2S by hydrogen is slow even at high temperatures and not likely to result in significant regeneration since the elution curves are exponential.

APPENDIX

Derivation of Sulfur Equilibrium Equations

The poisoning of a catalyst bed by sulfur may be thought of as a fixed-bed chromatographic operation. Sulfur may be ad-

sorbed or eluted from the bed by changing feed conditions. This result allows sulfur equilibrium curves to be determined by saturating the catalyst bed with sulfur and then eluting the sulfur with a sulfur-free hydrogen stream.

The equation of continuity for a fixed-bed separation may be developed by making a material balance over a column segment Δz, for a solute A:

$$\text{(rate of } A \text{ in)} - \text{(rate of } A \text{ out)} = \text{rate of accumulation of } A. \quad (1)$$

The rate of transfer of A into the system at z is

$$\epsilon S[v_z C_A - D_{A_a}(\partial C_A/\partial z)\,|_z] \quad (2)$$

Here S is the cross section, ϵ is the void fraction, v_z is the fluid velocity, and C_A is the bulk gas concentration. The term D_{A_a} is the effective diffusity of this solute in the bed. Since mass leaves the system by the same mechanisms as it enters, the left side of Eq. (1) becomes

$$\epsilon S\{[v_z C_A - D_{A_a}(\partial C_A/\partial z)]\,|_z - [v_z C_A - D_{A_a}(\partial C_A/\partial z)]\,|_{z+\Delta z}\}. \quad (3)$$

The rate of accumulation of A within the system is

$$S\Delta z[\epsilon(\partial C_A/\partial t) + (1-\epsilon)(\partial C_{A_s}/\partial t)], \quad (4)$$

where C_{A_s} is the bed concentration of A. Combination of Eqs. (3) and (4) and division by $S\Delta z$ results in

$$D_{A_a}\{[(\partial C_A/\partial_z)\,|_{z+\Delta z} - (\partial C_A/\partial z)\,|_z]\}/\Delta z = v_z(C_A\,|_{z+\Delta z} - C_A\,|_z)/\Delta z + \{(\partial C_A/\partial t) + [(1-\epsilon)/\epsilon](\partial C_{A_s}/\partial t)\}. \quad (5)$$

Taking the limit as Δz approaches zero yields

$$D_{A_a}(\partial^2 C_A/\partial z^2) = v_z(\partial C_A/\partial z) + (\partial/\partial t) \times \{C_A + [(1-\epsilon)/\epsilon]C_{A_s}\}. \quad (6)$$

Equation (6) is the continuity equation for solute A in a fixed-bed operation. This equation may be simplified by assuming that no axial mixing occurs. This assumption yields

$$v_z(\partial C_A/\partial z) + (\partial/\partial t)[C_A + \{(1-\epsilon)/\epsilon\}C_{A_s}] = 0. \quad (7)$$

Multiplying Eq. (7) by ϵ and defining $(1-\epsilon)C_{A_s}$ as $\rho_B q_A$ results in

$$\epsilon\partial C_A/\partial t + \rho_B \frac{\partial q_A}{\partial t} + \epsilon v_z \frac{\partial C_A}{\partial z} = 0, \quad (8)$$

where ρ_B is the bulk density of the bed and q_A is the solid concentration per unit mass.

Equation (8) must be coupled with an equation representing the solid phase alone:

$$\rho_B \frac{\partial q_A}{\partial t} = kaF(C_A, q_A), \quad (9)$$

where ka is the interphase mass-transfer coefficient and $F(C_A, q_A)$ is the driving force.

If k is assumed to be very large, then the solid-phase concentration is always in equilibrium with the gas phase and hence,

$$q_A = q_A^* = f(C_A), \quad (10)$$

where $*$ denotes equilibrium and $f(C_A)$ is the equilibrium curve function. Since k is assumed to be large,

$$\frac{\partial q_A}{\partial C_A}\frac{\partial C_A}{\partial t} = f'(C_A)\frac{\partial C_A}{\partial t}. \quad (11)$$

Substituting Eq. (11) into Eq. (8) results in

$$\left[1 + \frac{\rho_B}{\epsilon} f'(C_A)\right]\frac{\partial C_A}{\partial t} + v_z \frac{\partial C_A}{z\partial x} = 0. \quad (12)$$

The equilibrium curve may be determined by solving Eq. (12) jointly with the total differential of concentration:

$$\left(\frac{\partial C_A}{\partial t}\right)dt + \left(\frac{\partial C_A}{\partial x}\right)dx = dC_A. \quad (13)$$

Equations (12) and (13) are two equations in two unknowns. Solving for $\partial C_A/\partial t$ results in

$$\frac{\partial C_A}{\partial t} = \frac{\begin{vmatrix} 0 & v_z \\ dC_A & dx \end{vmatrix}}{\begin{vmatrix} 1 + \frac{\rho_B}{\epsilon} f'(C_A) & v_z \\ dt & dx \end{vmatrix}}. \quad (14)$$

There are certain ratios dx/dt which make the denominator equal to zero. However, $\partial C_A/\partial t$ must remain bounded, which implies that dC_A is equal to zero. Hence, the characteristic equation for the bed is

$$\frac{dx}{dt} = 1 + \frac{v_z}{(\rho_B/\epsilon) f'(C_A)}. \qquad (15)$$

Integrating the previous equation will allow solution of the equilibrium curve. The integrated equation is

$$x/t = \frac{v_z}{1 + (\rho_B/\epsilon) f'(C_A)}. \qquad (16)$$

Solving for $f'(C_A)$ results in

$$f'(C_A) = \frac{dq_A^*}{dC_A} = \frac{\epsilon}{\rho_B}\left(\frac{v_z t}{x} - 1\right). \qquad (17)$$

From Eq. (17), the slope of the equilibrium curve is determined as a function of time. Noting, however, that the elution curve relates time to concentration, dq_A^*/dC_A is known as a function of concentration. The integration of dq_A^*/dC_A with respect to concentration results in

$$f(C_A) = \int_{c_1}^{c_2} \frac{dq_A^*}{dC_A}\, dC_A, \qquad (18)$$

which is the desired equilibrium curve assuming local equilibrium through the bed.

ACKNOWLEDGMENTS

The authors gratefully acknowledge technical assistance by Dr. Charles Pitt (Department of Metallurgical, Mining and Fuels Engineering, University of Utah) and Dr. Bernard J. Wood (Stanford Research Institute) in providing X-ray diffraction and Auger analysis, and support of this work by the National Science Foundation (ENG75-00254). We also express gratitude to Professor Michel Boudart (Stanford), Dr. Jon G. McCarty (Stanford Research Institute), and Dr. John Falconer (University of Colorado) for providing very helpful comments and suggestions in regard to the manuscript.

REFERENCES

1. Mills, G. A., and Steffgan, F. W., *Catal. Rev.* **8**, 159 (1973).
2. Vannice, M. A., *Catal. Rev.* **14**, 153 (1976).
3. Dalla Betta, R. A., Piken, A. G., and Shelef, M., *J. Catal.* **40**, 173 (1974).
4. Perdereau, M., and Oudar, J., *Surface Sci.* **20**, 80 (1970).
5. Rostrup-Nielsen, J. R., *J. Catal.* **11**, 220 (1968).
6. Richardson, J. R., *J. Catal.* **21**, 130 (1970).
7. Rosenqvist, T., *J. Iron Steel Inst.* **176**, 37 (1954).
8. Roberts, M. W., *Nature (London)* **188**, 1020 (1960).
9. Rostrup-Nielsen, J. R., *J. Catal.* **21**, 171 (1971).
10. Den Besten, I. E., and Selwood, P. W., *J. Catal.* **1**, 93 (1963).
11. Saleh, J. M., Kemball, C., and Roberts, M. W., *Trans. Faraday Soc.* **57**, 1771 (1961).
12. Bartholomew, C. H., and Farrauto, R. J., *J. Catal.* **45**, 41 (1976).
13. Sherwood, T. K., Pigford, R. L., and Wilke, C. R., "Mass Transfer," pp. 554–561. McGraw-Hill, New York, 1975.
14. Lightfoot, E. N., Sanchez-Palma, R. J., and Edwards, D. O., "Separation Techniques" (H. M. Schoen, Ed.), pp. 99–182, Interscience, New York, 1962.
15. Zutshi, P. K., and Mahadevan, T. N., *Talanta* **17**, 1014 (1970).
16. Gustafsson, L., *Talanta* **4**, 227 (1960).
17. Gustafsson, L., *Talanta* **4**, 236 (1960).
18. Pannell, R. B., Chung, K. S., and Bartholomew, C. H., *J. Catal.* **46**, 340 (1977).
19. Somorjai, G. A., *J. Catal.* **27**, 453 (1972).
20. Benard, J., *Catal. Rev.* **3**, 93 (1969).
21. Edmonds, T., McCarroll, J. J., and Pitketh, R. O., *J. Vac. Sci. Technol.* **8**, 68 (1971).
22. Martin, G., and Imelik, G., *Surface Sci.* **42**, 157 (1974).
23. Bartholomew, C. H., "Alloy Catalysts with Monolith Supports for Methanation of Coal-Derived Gases." Annual Technical Progress report to ERDA, FE-1790-4, May 6, 1976.
24. Bartholomew, C. H., "Alloy Catalysts with Monolith Supports for Methanation of Coal-Derived Gases." Quarterly Technical Progress Report to ERDA, FE-1790-8, May 6, 1977.
25. Novak, E. J., and Koros, R. M., *J. Catal.* **7**, 50 (1967).
26. Wood, B. J., and Bartholomew, C. H., unpublished results.
27. Angevine, P. J., and Delgass, W. N., submitted to I & EC Fund.
28. Bartholomew, C. H., "Alloy Catalysts with Monolith Supports for Methanation of Coal-Derived Gases." Quarterly Progress Reports to ERDA, FE-1790-5, August 6, 1976.
29. Glass, R. W., and Ross, R. A., *J. Phys. Chem.* **77**, 2576 (1973).
30. Demuth, J. E., Jepson, D. W., and Marcus, P. M., *Phys. Rev. Lett.* **32**, 1182 (1974).
31. Reed, T. M., and Gibbins, K. E., "Applied Statistical Mechanics." McGraw-Hill, New York, 1973.